processes

MDPI

Article

Comparative Analysis of Weighting-Factor-Free Predictive Control Strategies for Direct Torque Control in Permanent Magnet Synchronous Machines

Jakson Bonaldo [1], Jacopo Riccio [2], Emrah Zerdali [3], Marco Rivera [2,4,*], Raul Monteiro [1] and Patrick Wheeler [2]

[1] Department of Electrical Engineering, Federal University of Mato Grosso, Avenida Fernando Correa da Costa, 1367, Cuiaba 78060-900, Brazil; jakson.bonaldo@ufmt.br (J.B.); raul.monteiro@ufmt.br (R.M.)
[2] Power Electronics, Machines and Control (PEMC) Research Institute, Department of Electrical and Electronic Engineering, Faculty of Engineering, University of Nottingham, 15 Triumph Rd, Lenton, Nottingham NG7 2GT, UK; jacopo.riccio@nottingham.ac.uk (J.R.); pat.wheeler@nottingham.ac.uk (P.W.)
[3] Department of Electrical and Electronics Engineering, Ege University, Izmir 35040, Türkiye; emrah.zerdali@ege.edu.tr
[4] Laboratorio de Conversión de Energías y Electrónica de Potencia (LCEEP), Vicerrectoría Académica, Universidad de Talca, 2 Norte # 685, Talca 3460000, Chile
* Correspondence: marco.rivera@nottingham.ac.uk

Abstract

Direct torque control (DTC) based on the finite control set model predictive control (FCS-MPC) provides a straightforward and intuitive solution for controlling permanent magnet synchronous motors (PMSMs). However, conventional FCS-MPC relies on appropriately tuned weighting factors in the cost function, which have a significant impact on the control performance and increase design complexity. This paper presents a comprehensive experimental comparison of emerging FCS-MPC strategies for DTC of PMSMs that eliminate the need for weighting factors. Specifically, a sequential FCS-MPC approach is benchmarked against decision-making-based FCS-MPC methods that employ Euclidean distance normalisation. Extensive experimental results, obtained across a wide range of operating conditions, are used to assess current total harmonic distortion (THD), torque and flux ripple, and transient performance. Results indicate that while all methods yield comparable current THD, decision-making-based strategies achieve superior torque and flux regulation with reduced ripple compared to the sequential approach. These findings demonstrate that decision-making-based FCS-MPC methods provide additional flexibility in defining control objectives, eliminating the need to design weighting factors, such as those used in the sequential method while offering superior performance.

Keywords: decision-making MPC; direct speed predictive control; finite control set-model predictive control; permanent magnet synchronous motor; sequential MPC

Academic Editor: Hsin-Jang Shieh

Received: 3 July 2025
Revised: 11 August 2025
Accepted: 14 August 2025
Published: 18 August 2025

Citation: Bonaldo, J.; Riccio, J.; Zerdali, E.; Rivera, M.; Monteiro, R.; Wheeler, P. Comparative Analysis of Weighting-Factor-Free Predictive Control Strategies for Direct Torque Control in Permanent Magnet Synchronous Machines. *Processes* **2025**, *13*, 2614. https://doi.org/10.3390/pr13082614

1. Introduction

Due to characteristics such as high power and torque density, compact size, and high power factor, permanent magnet synchronous motors (PMSMs) are widely used in high-performance electrical drive applications [1]. Regarding control methods, Field-Oriented Control (FOC), introduced in the early 1970s, has become the standard strategy for controlling electrical machines in industrial applications, electromobility, and energy conversion systems using voltage source inverters (VSIs) as the drive system [2]. The FOC strategy

enables nominal torque performance at low rotation speeds while also offering a wide speed range and independent control of speed and torque.

However, it relies on traditional cascaded linear controllers, which require the linearisation of both the machine and drive models. This process involves a carefully designed controller. It is limited by bandwidth, which can compromise the system's dynamic response throughout the current operating region, especially for strong back electromotive force (BEMF) harmonics and torque ripple characteristics [3]. In contrast, direct torque control (DTC) offers a faster transient response, is less sensitive to motor parameter variations compared to FOC, ensures consistent dynamic performance regardless of the operating point, and simplifies the control system design. However, it exhibits high current harmonics and significant fluctuations in torque and flux due to inner hysteresis controllers [4].

Advancements in the processing power of modern microprocessors have led to the development of various control techniques for PMSM drive systems. These techniques aim to improve the dynamic behaviour of speed and torque, as well as to improve steady-state performance [5,6]. Among them, Model Predictive Control (MPC) has attracted attention for its effectiveness in handling nonlinear systems, its ability to track multiple control objectives, its rapid transient response, and its straightforward implementation, especially in the context of the finite control set model predictive control (FCS-MPC) strategy [7,8]. Despite the advantages presented, some issues remain open and represent research opportunities on parameter dependency, high torque fluctuations, high current harmonics, variable switching frequency, high computational requirements, and difficulty in selecting suitable weighting factors (WFs) [9].

Conventional FCS-MPC employs a single cost function with weighting factors to address additional control objectives, specifically the controlled variables. However, the selection of weighting factors regarding a specific control objective significantly affects the remaining controlled variables [10], as in many cases, the target objectives may require conflicting actions [11]. In other words, if a high weighting factor is applied to achieve a given objective, the other control variables may deviate from the target reference. The above discussion enforces that the values of the weighting factor directly influence the performance of the system. However, it is not simple to define suitable weighting factor values to achieve the desired behaviour of the system. Typically, the procedure involves a heuristic approach that defines individual merit figures, followed by numerous exhaustive simulations or experiments [12]. This approach often relies on the experience of engineers and is a time-consuming process [13].

In [14,15], an approach and a set of guidelines are presented to reduce uncertainty and time consumed in defining weighting factors, relying on the classification of different types of cost functions and weighting factors. Despite this attempt to systematise the weighting factor designs, a high number of simulations is still required. To overcome the challenges related to the design of weighting factors, various FCS-MPC strategies have been proposed in recent years, including homogeneous control variables [16], FCS-MPCs based on direct vector selection [17], sequential model predictive control (S-MPC), and FCS-MPCs based on decision-making (DM).

A conventional S-MPC has been shown to exhibit instability throughout the operating speed range when the stator flux linkage cost function is prioritised during the sequential evaluation process in direct torque control of the induction motor [18]. A generalised S-MPC (GS-MPC) framework has been introduced to overcome this limitation. The proposed method ensures robust performance regardless of the execution order of the torque- and flux-related cost functions. Compared to the conventional approach, the GS-MPC achieves a reduced stator flux ripple, a lower total harmonic distortion (THD) of the current, and a decreased average switching frequency. Similarly, the order in which individual cost

functions are evaluated, that is, primary and secondary control objectives, was addressed in [19], considering a PMSM drive.

It shows that choosing torque as the primary cost function improves the current THD and torque ripple. The S-MPC strategy proposed in [20] selects the optimal switching vector based on the minimum cross-error among all control objectives. This technique avoids defining a priority control objective at the cost of a slightly higher computational burden than conventional S-MPC, since all cost functions are calculated for all switching vectors.

In [21], a lexicographic S-MPC method is proposed to eliminate the weighting factors that are typically used to control the torque and flux of PMSMs in direct torque control approaches. The technique relies on defining a tolerance value for the primary cost function to dynamically adjust the number of candidate voltage vectors to be applied to evaluate the secondary control objective. In addition to this methodology, to avoid presetting the number of candidate vectors, the tolerance band must still be carefully designed to ensure the proper functioning of the strategy. Similarly, the work presented in [22] also proposes using tolerance bands in an S-MPC approach to avoid weighting factors or manually selecting the number of candidate vectors. Unlike [21], the tolerance band is adjusted online based on the torque boundaries by applying a zero-voltage vector to avoid instantaneous increases in torque beyond the tolerance band. The torque boundaries are predicted using gradient functions, increasing the complexity and computational burden of this method.

On the other hand, various decision-making (DM) methods have been proposed to eliminate weighting factors in FCS-MPC strategies, particularly for model predictive torque control, over the last decade [23–40]. These techniques formulate the optimisation problem in a multi-objective way by evaluating each voltage vector for each control objective individually. Subsequently, a voltage vector selection algorithm, a key component of DM-based methods, selects the optimal voltage vector based on all control objectives.

The ranking-based DM method proposed in [23] evaluates each voltage vector separately with respect to torque and flux objectives, assigning ranking values based on the increasing values of the cost function. The vector with the lowest average rank is selected and applied to the VSI. However, this method faces high computational complexity, particularly when incorporating secondary control objectives, due to the sorting algorithm required. To address this, a hybrid sorting method was developed in [24], reducing the computational load. However, it assumes equal importance for each objective, which can lead to imbalanced control and instability, as demonstrated in [25]. A top-three voltage vector method in [26] considers the best three candidates for each objective and selects their intersection, but it does not address the case when there is no common vector. Further alternative DM approaches proposed in the literature include the VIKOR method [27], fuzzy-based DM [28], TOPSIS [29,30], coefficient of variation [31], grey relational analysis [32,33], and the weighted sum approach [34,35].

The Euclidean and absolute value norm-based methods presented in [36] achieve a balance between dynamic performance and computational simplicity and thus represent a practical alternative to the approaches discussed above. The Euclidean norm DM was also applied to model predictive direct speed control (MPDSC) in [37]. An equivalent WF method in [38] achieved lower torque and flux ripple than ranking-based DM with reduced complexity. In [41], a comparison of the elimination techniques of the weighting factor applied to the predictive torque control scheme of an induction motor was carried out, focussing on the primary control objectives—torque and flux—and highlighting aspects such as design complexity, computational burden, and effectiveness in achieving these objectives.

Considering these research opportunities, the present work aims to broaden the discussion on FCS-MPC applications of direct torque control to PMSMs without using weighting factors. Therefore, the performance of the standard S-MPC method and the decision-making MPC methods is comprehensively compared in terms of torque ripple, flux ripple, total harmonic distortion (THD) of currents, average switching frequency, processing time, and implementation complexity. The selection of the methods for the comparative analysis was motivated by the recent interest in weighting-factor-free MPC approaches. In addition, the methods were chosen such that all control strategies share the non-constant switching frequency nature, which is critical to ensure consistent and comparable results. The results are discussed in depth, considering a specific operating point, followed by a comprehensive performance assessment that considers a broad range of operating points. The analysis of the comprehensive performance assessment provides designers with subsidies to choose the weighting factorless approach that best fits a given application of PMSM direct torque control.

The main contributions of the present work are summarised below.

- Provides a comprehensive performance assessment among weighting-factorless FCS-MPC strategies, highlighting performance indices such as current THD, torque and flux ripple, average switching frequency, and implementation complexity.
- Highlights the suboptimal control performance associated with the S-MPC strategy applied to direct torque control of PMSMs and shows that the decision-making strategies are suitable approaches to weighting-factorless FCS-MPC controllers.
- Provides a step-by-step guide to the implementation of S-MPC and DM strategies aiming to control AC drive systems based on PMSMs.

The rest of this paper is organised as follows. Section 2 briefly discusses the DTC approach and the PMSM model, including equations in continuous and discrete time. The outer loop control based on a proportional–integral (PI) controller used to generate the torque reference is discussed and designed in Section 3. Section 4 presents the sequential and decision-making FCS-MPC strategies used to implement direct torque control. Section 5 presents the experimental results and a performance comparison between the control strategies at a specific operating point. Section 6 provides a comprehensive performance assessment that considers key indicators and several operating points. Finally, Section 7 concludes the paper with a summary of key findings.

2. Model of PMSM and Drive System

The permanent magnet synchronous motor model can be represented in state-space form such as shown in (1), where $\boldsymbol{A}_1$, $\boldsymbol{B}_1$, and $\boldsymbol{D}_1$ represent the system matrix, input matrix, and disturbance vector, respectively. The nonlinear behaviour of the PMSM becomes evident when the system is expanded, considering the values of the system's matrices as defined in (2). The electrical model is defined using the synchronous reference frame (dq), resulting in the states (di_d/dt) and (di_q/dt).

$$\frac{d}{dt}\boldsymbol{x}(t) = \boldsymbol{A}_1\boldsymbol{x}(t) + \boldsymbol{B}_1\boldsymbol{u}(t) + \boldsymbol{D}_1 \tag{1}$$

$$\frac{d}{dt}\begin{bmatrix} i_d \\ i_q \\ \omega_m \end{bmatrix} = \underbrace{\begin{bmatrix} -\frac{R_s}{L_d} & \frac{L_q p_p}{L_d}\omega_m & 0 \\ -\frac{L_d p_p}{L_q}\omega_m & -\frac{R_s}{L_q} & -\frac{\psi_f p_p}{L_q} \\ 0 & \frac{3}{2}\frac{\psi_f p_p}{J} & -\frac{B}{J} \end{bmatrix}}_{\boldsymbol{A}_1}\begin{bmatrix} i_d \\ i_q \\ \omega_m \end{bmatrix} + \underbrace{\begin{bmatrix} \frac{1}{L_d} & 0 \\ 0 & \frac{1}{L_q} \\ 0 & 0 \end{bmatrix}}_{\boldsymbol{B}_1}\begin{bmatrix} v_d \\ v_q \end{bmatrix} + \underbrace{\begin{bmatrix} 0 \\ 0 \\ -\frac{1}{J}T_L \end{bmatrix}}_{\boldsymbol{D}_1} \tag{2}$$

with the parameters defined as:

- R_s: stator resistance;
- L_d, L_q: stator inductances modeled on the dq-axis;
- v_d, v_q: stator voltages on the dq-axis;
- i_d, i_q: stator currents on the dq-axis;
- ω_m: mechanical speed;
- ψ_f: permanent magnet flux linkage;
- p_p: number of pole pairs;
- J: total inertia;
- B: viscous friction coefficient;
- T_L: load torque.

FCS-MPC strategies directly use the discretised system model to predict the future behaviour of the states. Then, employing the Euler first-order forward approximation given by (3), the stator currents can be predicted using the mathematical model in (4) and (5). T_s is the sampling time, and $L_d = L_q = L_s$ for a surface-mounted PMSM.

$$\frac{dx}{dt} \approx \frac{x_{k+1} - x_k}{T_s}, \tag{3}$$

$$i_{d,k+1} = i_{d,k} + T_s\left(\frac{v_{d,k}}{L_s} - \frac{R_s}{L_s} i_{d,k} + p_p \omega_{m,k} i_{q,k}\right) \tag{4}$$

$$i_{q,k+1} = i_{q,k} + T_s\left(\frac{v_{q,k}}{L_s} - \frac{R_s}{L_s} i_{q,k} - p_p \omega_{m,k} i_{d,k} - \frac{p_p}{L_s}\psi_f \omega_{m,k}\right) \tag{5}$$

Using (4) and (5), it is possible to predict the stator fluxes ($\psi_{d,k+1}$ and $\psi_{q,k+1}$):

$$\psi_{d,k+1} = L_s i_{d,k+1} + \psi_f, \tag{6}$$

$$\psi_{d,k+1} = L_s i_{q,k+1}. \tag{7}$$

Consequently, the predicted electromagnetic torque ($T_{e,k+1}$) can be calculated using the predicted stator currents and fluxes as follows:

$$T_{e,k+1} = \frac{3}{2} p_p \left(\psi_{q,k+1} i_{d,k+1} - \psi_{d,k+1} i_{q,k+1}\right) \tag{8}$$

A two-level voltage source inverter (2L-VSI) can be used to supply the PMSM. In this case, the inverter output voltage vector can be defined in the stationary reference ($\alpha\beta$) frame as

$$\boldsymbol{v}_{s,\alpha\beta} = \frac{2}{3} V_{dc}(S_a + \boldsymbol{a} S_b + \boldsymbol{a}^2 S_c) \tag{9}$$

where V_{dc} is the dc-link voltage, $S_x \in \{S_a, S_b, S_c\}$ shows the switching states of the upper switches on each leg, and $\boldsymbol{a} = e^{-j120}$ is the 120 electrical degree phase change operator. For the given inverter topology, (9) yields seven different voltage vectors within the eight switching combinations that are possible to synthesise, as presented in Table 1.

The $\boldsymbol{v}_{s,\alpha\beta}$ can then be transformed into the $dq-$frame:

$$\boldsymbol{v}_{s,dq} = \boldsymbol{v}_{s,\alpha\beta} e^{-j\theta_r} \tag{10}$$

where θ_r is the electrical position of the PMSM rotor.

Table 1. Inverter switching states.

j	S_1	S_3	S_5	$v_{i\alpha}$	$v_{i\beta}$
1	1	0	0	$\frac{2}{3}V_{dc}$	0
2	1	1	0	$\frac{1}{3}V_{dc}$	$\frac{\sqrt{3}}{3}V_{dc}$
3	0	1	0	$-\frac{1}{3}V_{dc}$	$\frac{\sqrt{3}}{3}V_{dc}$
4	0	1	1	$-\frac{2}{3}V_{dc}$	0
5	0	0	1	$-\frac{1}{3}V_{dc}$	$-\frac{\sqrt{3}}{3}V_{dc}$
6	1	0	1	$\frac{1}{3}V_{dc}$	$-\frac{\sqrt{3}}{3}V_{dc}$
7	1	1	1	0	0
8	0	0	0	0	0

3. Speed Controller Design

Direct torque control relies on a cascade control structure composed of an internal control loop used to regulate the measured torque according to the torque reference. The internal loop commonly uses proportional–integral (PI) controllers or hysterisis controllers. The outer loop yields the torque reference from the error between the speed reference and the measured speed.

A PI controller is typically used in the outer speed control loop, assuming that the inner control loop is properly designed and can be modelled as having a unit gain. Then, the design of the PI controller can be performed based on the mechanical equations of the PMSM, which are derived from (2) and represented in (11):

$$\frac{d\omega_m}{dt} = \frac{1}{J}\left(\frac{3}{2}p_p\psi_f i_q - T_L - B\omega_m\right), \tag{11}$$

where the electromagnetic torque (T_e) generated by the PMSM is represented by

$$T_e = \frac{3}{2}p_p\psi_f i_q. \tag{12}$$

By replacing (12) with (11) and applying the Laplace transform, the transfer function between the electromagnetic torque and the speed is defined as

$$\frac{\omega_m(s)}{T_e(s)} = \frac{1}{B + Js}. \tag{13}$$

The gains of the PI controller, whose transfer function is given by (14), can be designed based on the desired damping ratio (ζ) and the undamped natural frequency (ω_n) of the closed-loop system by comparing the canonical second-order transfer function, as shown in Equations (15) and (16).

$$\frac{\omega_m(s)}{T_e(s)} = k_p + \frac{k_i}{s} \tag{14}$$

$$k_p = 2J\omega_n\zeta - B \tag{15}$$

$$k_i = J\omega_n^2 \tag{16}$$

4. Model Predictive Controllers

Once the outer control loop generates the torque reference (T_e^*), the inner controller must ensure proper tracking of this reference. In the present research, three weightless FCS-MPC inner torque controllers are compared: (a) S-MPC, (b) decision-making MPC (DM), and (c) a subvariant of decision-making, including an additional control objective to decrease the switching effort (DM-SE). The description of each technique is presented below according to the control system overview presented in Figure 1.

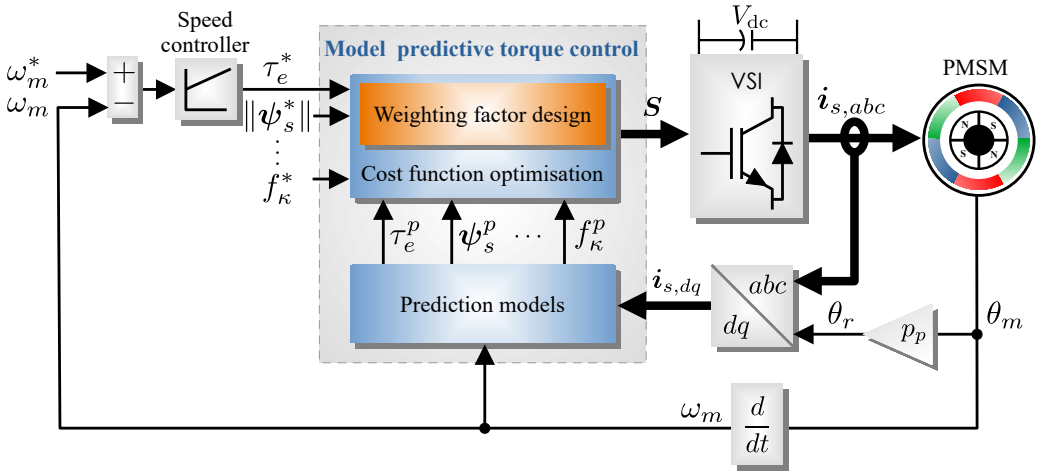

Figure 1. Block diagram of a PMSM fed by an FCS-MPC direct torque-controlled 2L VSI.

4.1. Sequential Model Predictive Control (S-MPC)

The S-MPC addressed in this work was first proposed in [42] to avoid the design complexity associated with the weighting factors. This strategy uses a sequential structure with a single cost function for each control objective. In the case of three-phase two-level VSI, the primary cost function is evaluated considering all the possible switching vectors (eight). Then a given number (N) of candidate switching vectors that produce the best value for the primary control cost function are ranked and used to evaluate the secondary cost function. In the end, a switching vector that complies with the restriction of all cost functions is selected and applied to the inverter. As highlighted in [18], the primary cost function has a higher priority over the secondary one. Despite its simplicity in design, the method requires a simplified adjustment process to define the optimum value of N.

The flow chart of Figure 2 details the implementation of the S-MPC direct torque control. Firstly, the stator currents in the $dq-$ reference frame are estimated to compensate for the delay using Equations (4) and (5) and the optimal voltage vector (v_{dq}^{opt}) from the previous control cycle. In S-MPC, the primary control objective is achieved by evaluating the cost function for the eight VSI voltage vectors in Table 1. Since the primary cost function aims to drive the torque error to zero, the torque should be predicted first. The torque prediction relies on the prediction of the stator currents two samples ahead using (17)–(21), which are the shifted versions of the expression (4)–(7), and (12), respectively. The variables v_d^j and v_q^j represent each voltage vector of Table 1 transformed to the synchronous reference frame.

$$i_{d,k+2} = i_{d,k+1} + T_s\left(\frac{v_d^j}{L_s} - \frac{R_s}{L_s}i_{d,k+1} + p_p\omega_{m,k}i_{q,k+1}\right) \tag{17}$$

$$i_{q,k+2} = i_{q,k+1} + T_s\left(\frac{v_q^j}{L_s} - \frac{R_s}{L_s}i_{q,k+1} - p_p\omega_{m,k}i_{d,k+1} - \frac{p_p}{L_s}\psi_f\omega_{m,k}\right) \tag{18}$$

$$\psi_{d,k+2} = L_s i_{d,k+2} + \psi_f, \tag{19}$$

$$\psi_{d,k+2} = L_s i_{q,k+2}. \tag{20}$$

$$T_{e,k+2} = \frac{3}{2}p_p\left(\psi_{q,k+2}i_{d,k+2} - \psi_{d,k+2}i_{q,k+2}\right) \tag{21}$$

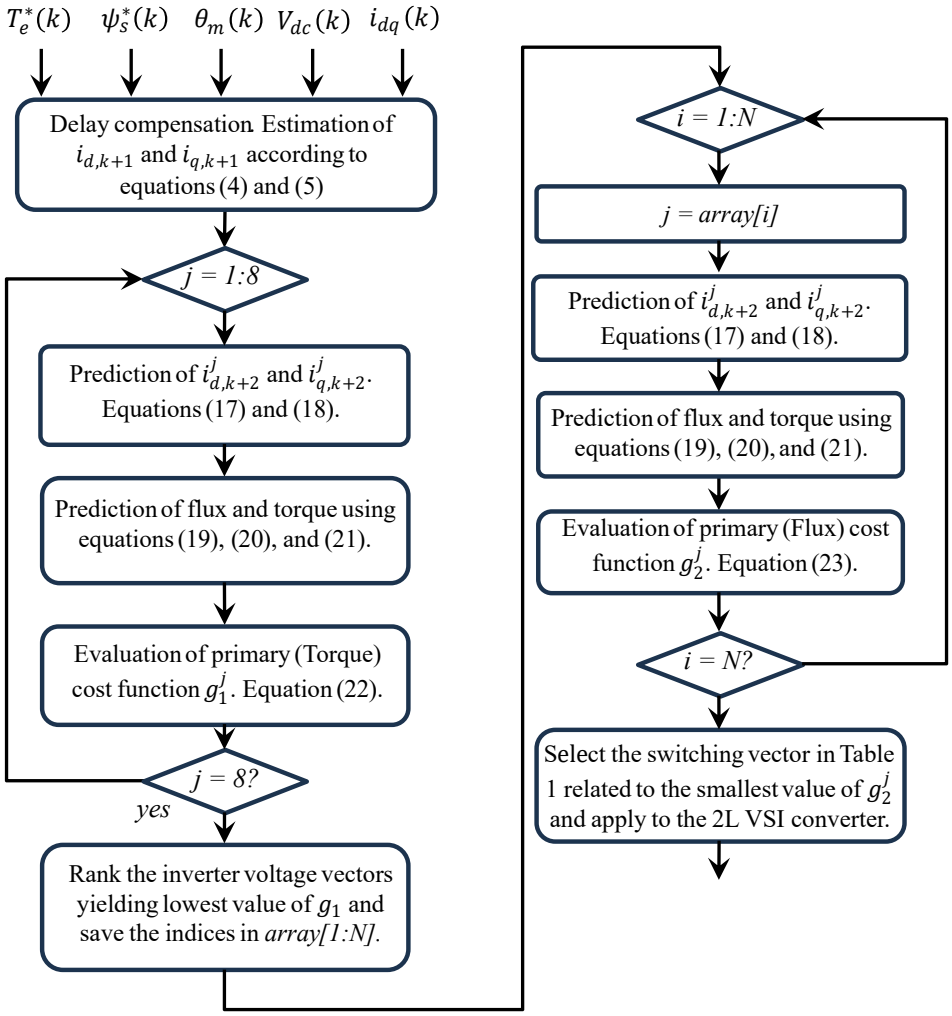

Figure 2. Flowchart of S-MPC approach.

Hence, the eighth values of primary cost function g_1^j, given by (22), are sorted in ascending order and an array with the indices of the switching states of Table 1 is created. Then, in the second stage of the S-MPC algorithm, the switching states corresponding to the first N positions of the sorted array are used to predict the stator currents and the flux linkage according to Equations (17)–(20).

Subsequently, the cost function related to the secondary control objectives g_2^j, defined in (23), is evaluated for each of the N pre-selected switching states. Finally, the optimal voltage vector (v_{dq}^{opt}) corresponding to the minimum-cost function value is selected and applied to the 2L VSI converter.

In order to suppress overcurrents and maintain the drive's operation safely, a constraint is combined in the cost functions to limit the magnitude of stator currents to the value $i_{s,max}$. Therefore, the primary cost function (g_1) can be defined by (25) and the secondary cost function (g_2) used to regulate the flux is given by (26).

$$g_1 = \left|T_e^* - T_{e,k+2}^p\right| + i_{oc,k+2}^p \tag{22}$$

$$g_2 = \left||\boldsymbol{\psi}_s^*| - |\boldsymbol{\psi}_{s,k+2}^p|\right| + i_{oc,k+2}^p \tag{23}$$

where

$$i_{\mathrm{oc},k+2}^p = \begin{cases} 0, & \text{if } |\boldsymbol{i}_{s,k+2}^p| \le i_{s,\max} \\ 1, & \text{if } |\boldsymbol{i}_{s,k+2}^p| > i_{s,\max} \end{cases}. \tag{24}$$

The S-MPC approach eliminates the need for weighting factors among objectives (i.e., flux and torque references) by restricting the feasible set of control inputs to ensure sequential dependency between the objectives, but this ultimately impacts overall optimality [15].

4.2. Decision-Making MPC

Many decision-based methods have been proposed in the literature, but the Euclidean norm-based DM proposed in [36] has a straightforward structure and lower computational complexity since it does not require a sorting algorithm.

4.2.1. Conventional Decision-Making MPC (DM-MPC)

DM-MPC evaluates each control objective independently and then uses a selection method to choose the optimal switching vectors. Consequently, this method eliminates the need to use WFs. However, instead of using a single cost function that considers all control objectives, the DM MPC method expresses the multiple objectives using separate equations, such as the S-MPC approach.

Since this work applies a DTC approach to control the PMSM speed, the primary control objective is defined as the torque cost function (25). The secondary control objective is to regulate the linkage flux (26).

$$g_1 = \left|T_e^* - T_{e,k+2}^p\right| \tag{25}$$

$$g_2 = \left||\boldsymbol{\psi}_s^*| - |\boldsymbol{\psi}_{s,k+2}^p|\right| \tag{26}$$

Furthermore, unlike the S-MPC approach, the current restriction is included as a separate control objective (27) to prevent permanent failures caused by overcurrent. Notice that (24) defines $i_{oc,k+2}^p$.

$$g_3 = i_{oc,k+2}^p \tag{27}$$

The following steps compose the proposed method:

Step 1: compensation of the delay in digital processing using Equations (4) and (5) to estimate the stator currents in the reference frame $dq-$ using the optimal voltage vector (v_{dq}^{opt}) from the previous control cycle.

Step 2: based on the estimated stator currents, the stator currents, flux, and torque are predicted using Equations (17), (18), (19), (20), and (21), respectively. This procedure produces the data required to compute the cost functions.

Step 3: by evaluating each cost function for each possible switching state, a dataset is constructed as follows:

$$\boldsymbol{X}_{ji} = \begin{pmatrix} g_1(\boldsymbol{v}_0) & g_2(\boldsymbol{v}_0) & \dots & g_n(\boldsymbol{v}_0) \\ g_1(\boldsymbol{v}_1) & g_2(\boldsymbol{v}_1) & \dots & g_n(\boldsymbol{v}_1) \\ \vdots & \vdots & \ddots & \vdots \\ g_1(\boldsymbol{v}_m) & g_2(\boldsymbol{v}_m) & \dots & g_n(\boldsymbol{v}_m) \end{pmatrix} \tag{28}$$

where $i \in \{1, 2, \dots, n\}$ indicates the number of control objectives and $j \in \{0, 1, \dots, m\}$ the number of switching vectors. Considering a 2L VSI, m represents the number of voltage vectors (eight) and, for the specific application proposed in this work, the number of control objectives is $n = 8$.

Step 4: normalise the dataset:

$$\boldsymbol{Y}_{ji} = \frac{\boldsymbol{x}_i^{\min} - x_{ji}}{\boldsymbol{x}_i^{\min} - \boldsymbol{x}_i^{\max}} \tag{29}$$

where $x_i^{\min}$ and $x_i^{\max}$ are the minimum and maximum values of each column vector x_i in X_{ji}.

Step 5: calculate the Euclidean norm in the $n-$dimensional space using the normalised dataset Y_{ji} for each switching vector:

$$d_j = ||y_j||_2 = \sqrt{\sum_{i=1}^{n} (y_{ji})^2} \tag{30}$$

where y_j refers to any row vector in Y_{ji}.

Step 6: select the jth switching vectors that minimises the d_j:

$$v_{\text{opt}} = \arg\min_j d_j \tag{31}$$

A detailed view of the DM algorithm is shown in the flow diagram in Figure 3, which summarises the procedures required by the DM MPC.

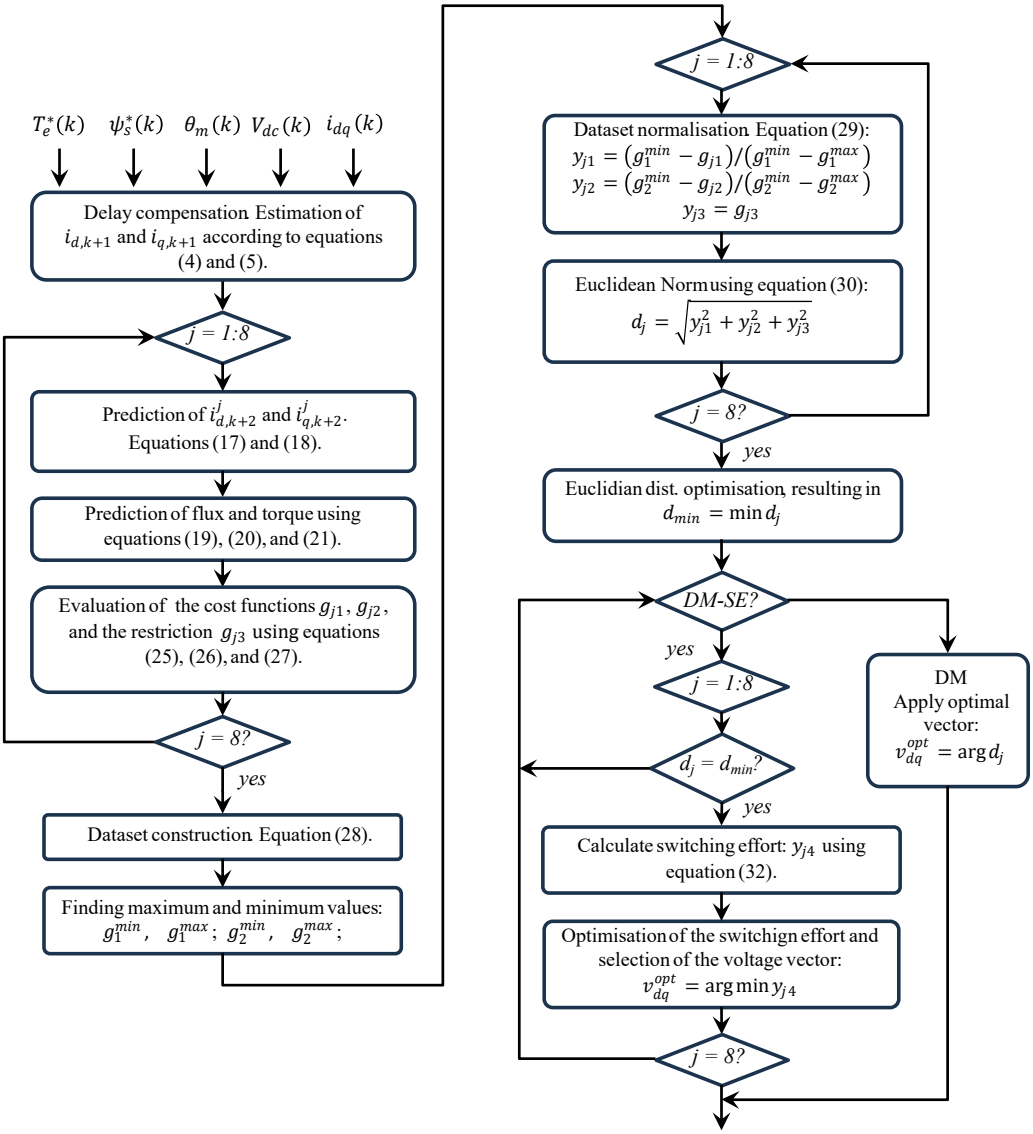

Figure 3. Flowchart of DM and DM-SE methods.

Like most WF design methods, this approach has limitations when incorporating secondary objectives, as it assumes that primary and secondary control objectives have a

similar impact on control performance. This limitation can lead to poor control performance or potential stability issues.

4.2.2. Decision-Making MPC with Additional Control Objective to Minimise the Switching Effort (DM-SE)

To address the aforementioned problems, ref. [36] proposed a cost-effective and flexible DM method that takes into account multiple control objectives, additional control objectives, and system constraints. The DM-SE method consists of two stages: (1) selecting l candidate voltage vectors for the second stage from options while accounting for system constraints and multiple objectives, and (2) selecting the ultimate optimal voltage vector based on additional control objectives from the candidates identified in the first stage (conventional DM). In essence, the method addresses the multiple objectives and the additional objectives in parallel while maintaining a sequential control structure between them. Its flexible architecture also allows for the number of hierarchical stages to be increased as needed for specific applications.

In the present paper, the additional control objective is to minimise the switching effort, which is achieved by reducing the switching frequency and thereby improving power losses. Therefore, based on the minimal value of the Euclidean norm given by (d_{min}) in the flow chart of Figure 3, the switching effort is evaluated according to (32) considering the eight switching states in Table 1 and the previous optimal switching state:

$$y_{j4} = |S_1^j - S_1^{opt}| + |S_3^j - S_3^{opt}| + |S_5^j - S_5^{opt}|, \tag{32}$$

where S_1^j, S_3^j, and S_3^j represent the switching state for the jth voltage vector, and S_1^{opt} are the optimal switching states used in the previous execution of the MPC algorithm.

Finally, the optimal voltage with the minimum Euclidean norm is selected and applied to the VSI.

It is important to highlight that the flow chart in Figure 3 represents both decision-making methods. When the variable *DM-SE* is false, the conventional DM algorithm is executed. On the other hand, when the *DM-SE* is true, the extended DM-SE method with switching frequency minimisation is executed.

5. Experimental Results

The effectiveness of the FCS-MPC approaches applied to the control of the 2L VSI feeding the PMSM presented in the previous sections is validated through experimental results. The performance of both discussed methods is evaluated under various operating conditions, considering potential operational scenarios of an AC drive. An overview of the setup of the control and drive systems discussed in this work is shown in the block diagram of Figure 1, which includes the control structure, power converter, and PMSM. The specifications of the former are listed in Table 2. The parameters used in the controllers are provided in Table 3. It is worth highlighting the difference between the average switching frequency and the instantaneous switching frequency within the presented MPCs. According to [15], the instantaneous switching frequency for a 28 kHz sampling frequency is 14 kHz. On the other hand, the average switching frequency varies with the operating conditions and is significantly lower than the instantaneous switching frequency. These parameters are considered constant and were experimentally verified using the no-load back electromotive force (EMF), given the importance of these parameters in determining the torque output [43].

The number of voltage vectors N used to evaluate the secondary objective (flux control) in the S-MPC approach was determined experimentally. For $N > 3$, the method becomes unstable due to poor torque regulation. When $N = 1$, the flux cost function cannot be

evaluated. The cases $N = 2$ and $N = 3$ yield comparable results, although flux ripple is slightly higher for $N = 2$. Therefore, the optimal number of voltage vectors for evaluating the secondary objective is $N = 3$.

The experimental setup is shown in Figure 4. The conventional MPTC and the proposed DM-based MPTC have been executed in real time with a sampling frequency of 28 kHz on the uCube platform based on the Zynq-7000 system on chip (AMD, Santa Clara, CA, USA) introduced in [44]. The uCube offers a compelling combination of versatility, user-friendly operation, and cost-effectiveness. In addition, it provides a seamless platform for implementing complex algorithms such as the proposed DM-based and sequential MPTC methods with exceptional flexibility and ease. In particular, the uCube uses the Avnet MicroZed system on module, which integrates a dual-core ARM Cortex-A9 (AMD, Santa Clara, CA, USA) (processor with programmable logic built on Xilinx Artix-7 FPGA (AMD, Santa Clara, CA, USA) technology. The test rig also includes the PMSM with the specifications in Table 2 as a controlled machine and a second PMSM used as a load machine. These machines are driven by two 2L-VSIs that share the same dc-link voltage. The inverter of the prime mover is an obsolete commercial drive customized with fiber optic interlinks to the control platform, while the inverter driving the machine under test (MUT) is based on an FS200R07N3E4R 650 V, 200 A six-pack IGBT module (Infineon Technologies, Neubiberg, Germany). The position feedback is acquired using an absolute encoder with a resolution of 17 bits. In addition, several 12-bit analog-to-digital converters are read by the programmable logic and used as feedback signals for the current and voltage measurements.

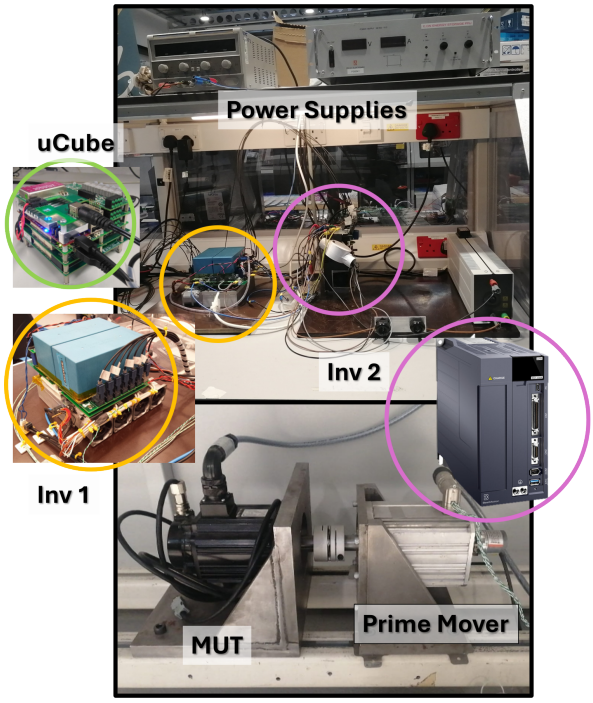

Figure 4. Overview of the experimental prototype.

Table 2. Specifications of the controlled PMSM.

Parameter	Value	Parameter	Value
P	2.0 kW	V_{dc}	300 V
n_m	3000 r/min	T_{rated}	6.36 N · m
p_p	4	ψ_f	0.067 V · s
R_s	0.80 Ω	L_s	2.2 mH
J_t	0.009 kg · m^2	B_t	0.0012 N · m · s

Table 3. Control parameters.

Description	Symbol	Value
Sampling frequency	F_s	28 kHz
Maximum allowable stator current limit	$i_{s,\max}$	12 A
Proportional gain of PI controller	k_p	2.5
Integral gain of PI controller	k_i	5000
Number of candidate voltage vectors (S-MPC)	N	3

Three different test scenarios are considered: a step change in load at constant speed, a step change in load with varying speed, and a speed reversal at constant torque load.

5.1. Torque Step Change Under Constant Speed

This test helps to understand how well the control system handles instantaneous changes in load while the motor continues to run at constant speed. In the first test scenario considered, the drive speed was set to a constant value of 2000 rpm using the prime mover (PM), and a torque step change of 4 Nm was applied to the MUT at approximately 170 ms. This test was performed at a dc-link voltage of 200 V, considering the S-MPC (see Figure 5a), the DM FCS-MPC without considering the switching effort (see Figure 5b), and the DM-SE FCS-MPC method addressing the switching effort (see Figure 5c). This scenario is analysed on the basis of the torque profile (top), the flux profile (middle), and the instantaneous currents (bottom). The flux reference is calculated from the torque reference assuming $i_d^* = 0$ to satisfy the maximum torque per ampere (MTPA) condition of a surface-mounted PMSM, as follows:

$$\psi^* = \sqrt{(\psi_d^*)^2 + (\psi_q^*)^2} = \sqrt{(\psi_f)^2 + (L_q i_q^*)^2} = \sqrt{\psi_f^2 + \left(L_q \frac{2T_{em}^*}{3p_p\psi_f}\right)^2} \tag{33}$$

It can be seen that the three approaches exhibit a similar dynamic torque response. The calculated average total harmonic distortion (THD) for the three-phase currents i_a, i_b, and i_c was similar between the three methods with 9.0% for S-MPC, 8.1% for conventional DM, and 8.4% for the DM-SE method including the minimisation of the switching effort. Furthermore, the resulting average switching frequency, calculated over one mechanical revolution, was 5.79 kHz, 5.57 kHz, and 4.85 kHz for the S-MPC, DM, and DM-SE, respectively. The torque ripple was 1.18 Nm, 1.26 Nm, and 1.16 Nm for S-MPC, DM, and DM-SE, respectively.

The DM-SE method was able to reduce by 20% the average switching frequency, thus reducing the power devices' switching losses whilst maintaining the THD and torque ripple consistent with S-MPC and conventional DM methods. Furthermore, both the DM and the DM-SE methods significantly reduced flux ripple as a result of their inherent objective optimisation. Due to the limited number of vectors used to evaluate the secondary objective in the S-MPC method (N = 3), the flux reference tracking is compromised. The following flux ripples, 12.8 mWb, 4.7 mWb, and 4.7 mWb, were obtained for S-MPC, DM, and DM-SE, respectively.

Finally, the torque request was step-changed from 4 Nm to 0 Nm, and the corresponding feedback results, calculated according to (21), are shown in Figure 5d. These results show the settling time for the direct torque control of 0.393 ms for the S-MPC, 0.357 ms for the DM, and 0.322 ms for the DM-SE method. The settling is consistent among the three approaches assessed, highlighting the fast transient response of the DTC allied to FCS-MPC methods.

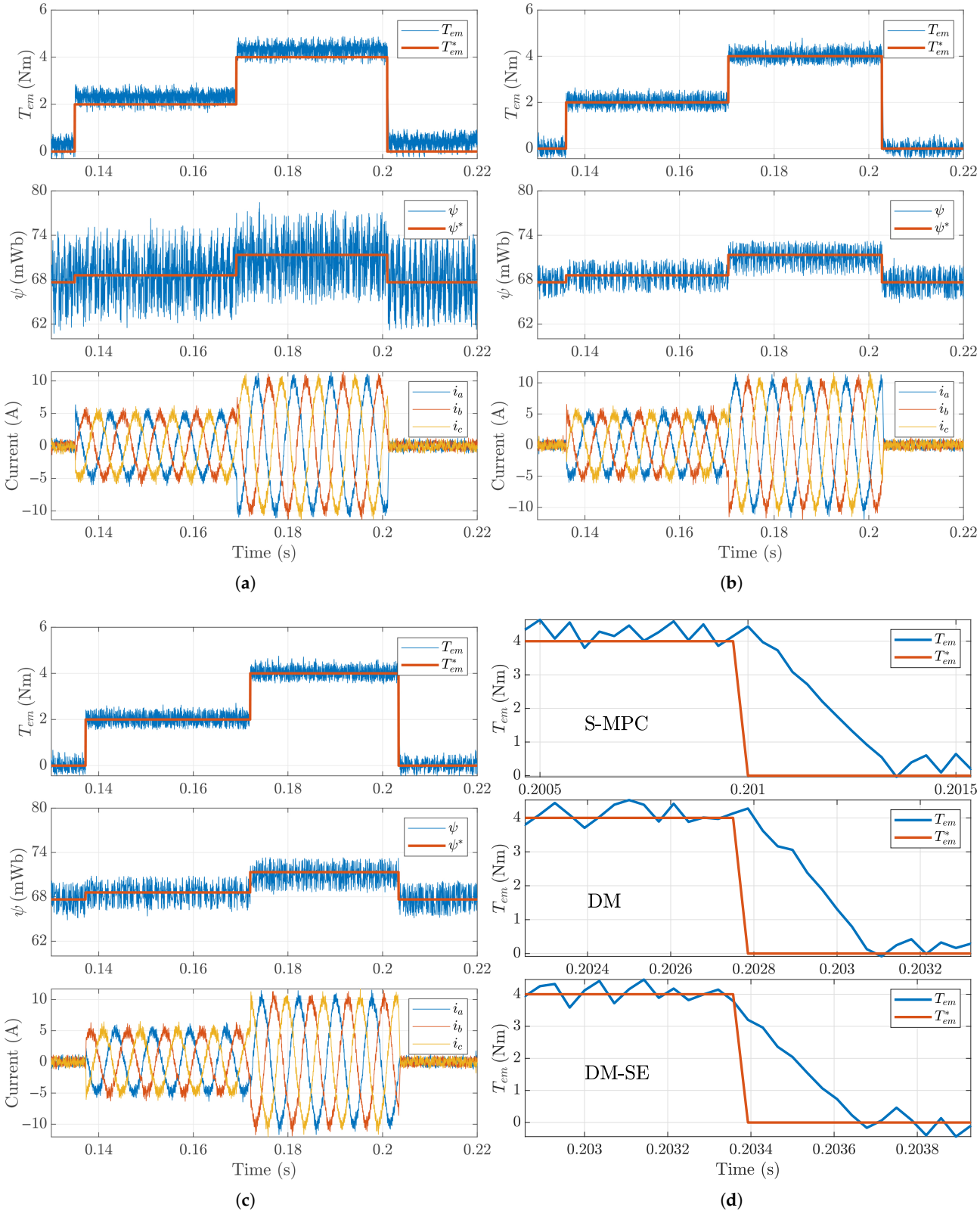

Figure 5. Torque, flux, and current waveforms for torque steps under constant speed (2000 rpm): (**a**) S-MPC; (**b**) DM; (**c**) DM-SE; (**d**) detail of torque step from 4 Nm to 0 Nm.

5.2. Speed Reversal Under Constant Torque

Further experimental tests were performed to validate the effectiveness of the proposed control method under speed reversal. Specifically, the drive speed was reversed from 2000 to −2000 rpm while maintaining a constant torque load of 3 Nm.

The results of this test are shown in Figure 6. The settling time for all the methods evaluated was 70 ms, highlighting the decoupled behaviour between the DTC provided by the FCS-MPC approaches and the linear speed control loop.

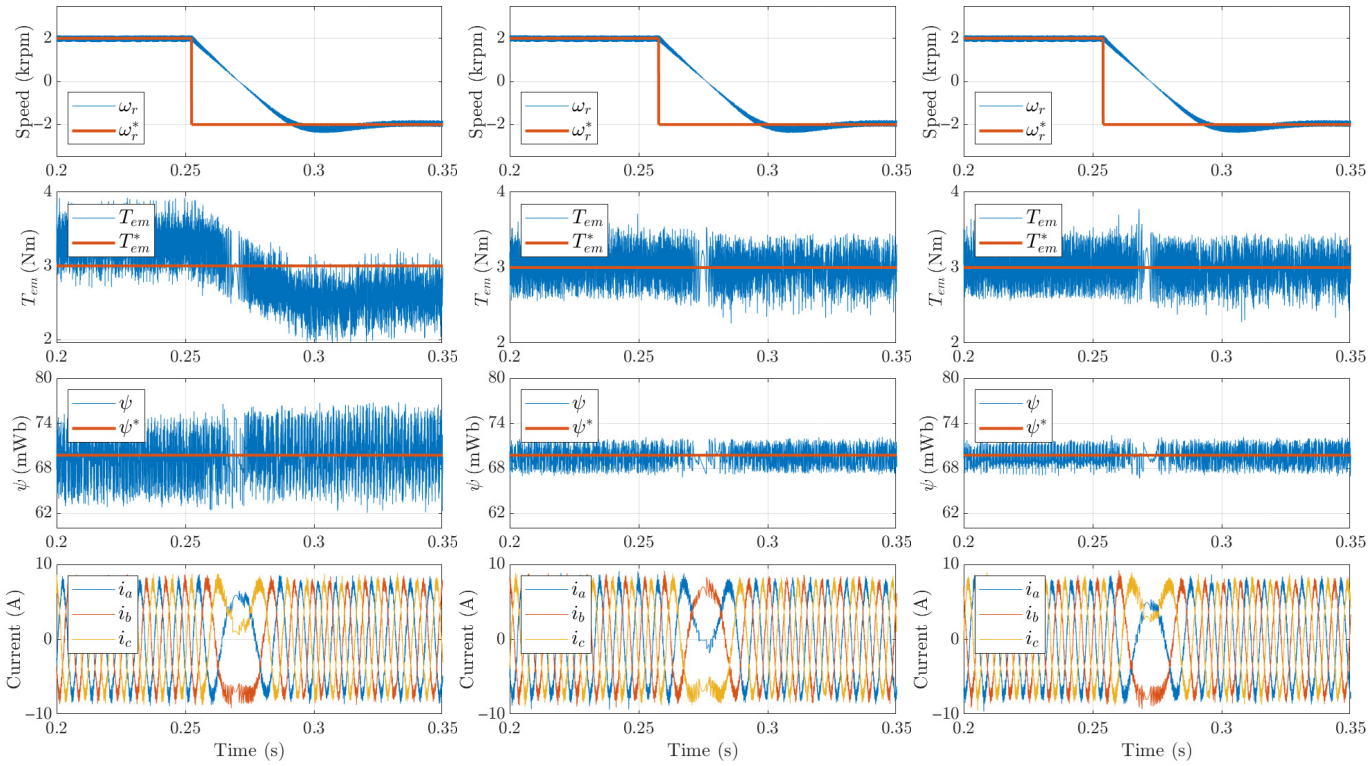

Figure 6. Speed reversal from 2000 rpm to −2000 rpm under constant torque of 3 Nm: (**a**) S-MPC; (**b**) DM; (**c**) DM-SE.

As seen in Figure 6a, the S-MPC methods experience some torque variation from an average value of 3.3 Nm to 2.7 Nm after the speed is reversed. Again, this behaviour could be attributed to the suboptimal solution provided by S-MPC, since the number of voltage vectors used to evaluate torque and flux does not provide enough granularity to achieve the optimal performance obtained by the DM methods. This is a direct consequence of the suboptimality introduced by the S-MPC, as also stated in [15]. The sequential approach overcomes the weighting factor selection challenge at the cost of suboptimal control across the various objectives, resulting in biased setpoint tracking and increased torque and flux ripples, which in turn lead to an overall higher current THD.

5.3. Load Step Change Under Varying Speed

An additional scenario considering operation with varying speed and load is proposed in this subsection to fully validate the performance of the assessed FCS-MPC methods under real conditions, and the results are reported in Figure 7. In this test, the PM machine starts with zero speed followed by a step of 1000 rpm under zero load. At approximately 0.08 s the load is increased to 4 Nm. At $t = 0.15$ an additional speed step change occurs increasing the speed to 2000 rpm. At $t = 0.27$ s the mechanical load is set back to zero, and at $t = 0.36$ s the speed decreases to 1000 rpm. The transient behaviour of the speed

loop shows a overshoot of 15 % for the three FCS-MPC methods with identical settling time of 60 ms for the speed change from 1000 rpm to 2000 rpm, and 40 ms for load changes.

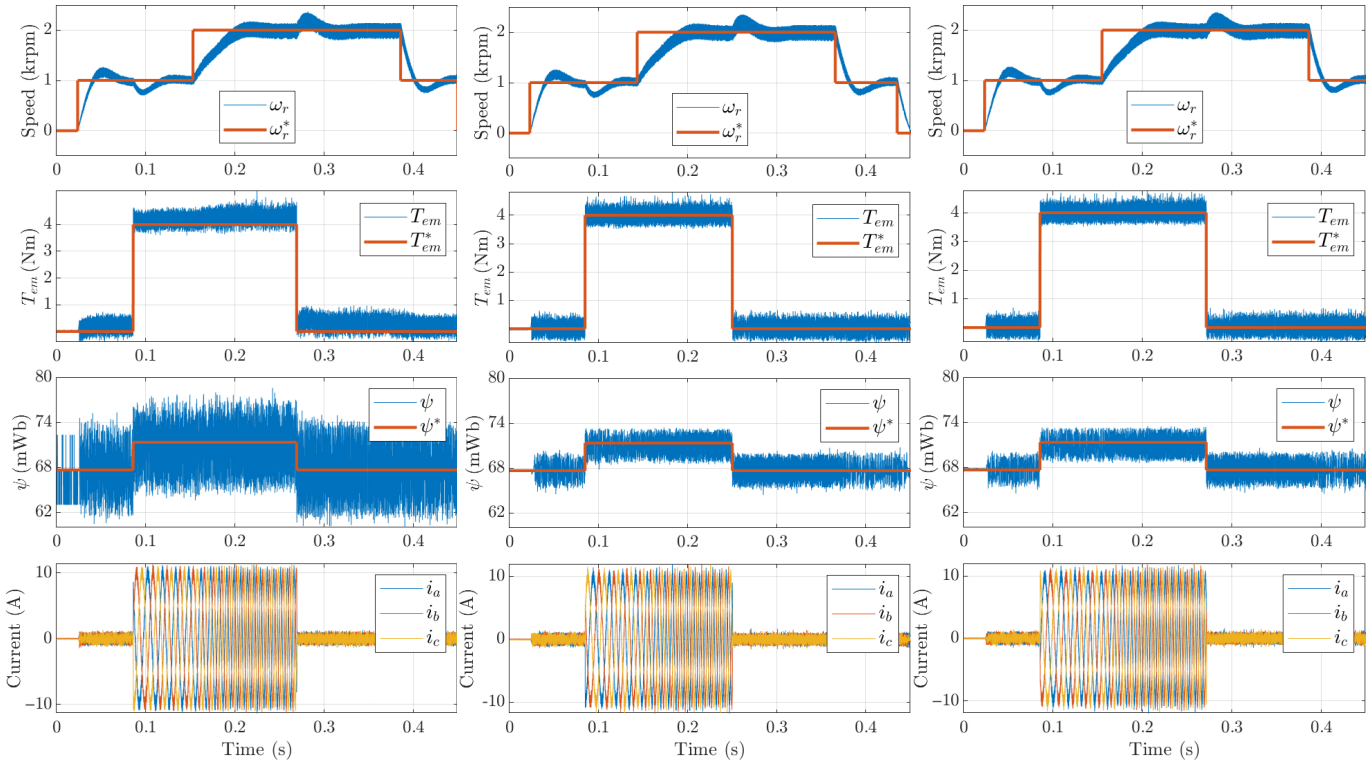

Figure 7. Speed incremental steps followed by load step change: (**a**) S-MPC; (**b**) DM; (**c**) DM-SE.

5.4. Computational Complexity

To verify the cost-effectiveness of the FCS-MPC methods evaluated and applied in direct torque control and to demonstrate the additional computational complexity caused by the DM methods, the execution times are presented in Table 4, considering the worst case observed during the experimental tests. The execution times presented in Table 4 focus on the execution of the MPC algorithms, disregarding the ADCs acquisition time and scaling of the measurements, such as shown in Figure 8. In particular, the end-to-end execution time was measured on the hardware platform described in [44] to estimate the worst-case execution time (WCET) following the guidelines reported in [45]. The predictable control flow, as illustrated by the flowchart in Figure 3, enables reliable and jitter-mitigated timing bounds. The *Ch4* represents the complete execution time of considering the ADC and digital signal preprocessing (t_1), the execution time of the MPTC algorithm (t_2), and the procedure for setting the digital outputs (to the power switches) and to store the measured data and preparing the function for the next interruption (t_3). On the other hand, the signal *Ch3* corresponds solely to the processing time of the MPTC algorithm. Note that two auxiliary IO ports were used to measure the execution times. The signal reaches a high level at the beginning of the function and then returns to a low level at the end.

Table 4. Execution times of MPTC strategies.

Method	Execution Time
S-MPTC	3.58 µs
DM	3.81 µs
DM-SE	3.95 µs

The computational complexity of MPTC increases slightly with the proposed DM-SE method due to the addition of the control objective used to reduce the switching frequency. The results indicate that the conventional DM and DM-SE methods have similar complexity and computation time. On the other hand, the computation time of the S-MPC method is approximately 10% lower than that of DM-SE when considering a two-level VSI and two cost functions. This difference tends to decrease with higher-level converters and an increased number of cost functions. However, the slightly higher computational burden of DM methods can be overlooked in considering improved control performance, design complexity, and flexibility in incorporating additional control objectives.

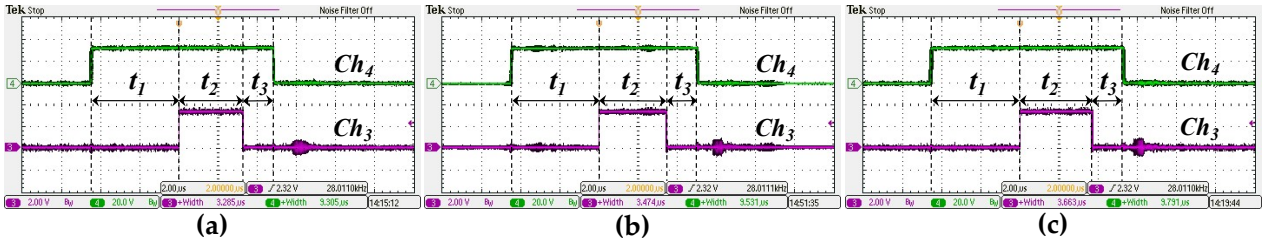

Figure 8. Measuring the execution time of the MPC approaches: (**a**) S-MPTC; (**b**) DM; and (**c**) DC-SE. Ch3 represents the execution time of the MPTC algorithm and Ch4 represents the execution time of the interruption routine used to process the ADC signals, preprocessing, and data collection.

Finally, Table 5 presents an estimation of the computational resource usage based on the Zynq-7000 microprocessor (AMD, Santa Clara, CA, USA), intended to serve as a reference for future implementations on other microcontrollers or microprocessors. The resource usage is divided into arithmetic operations such as addition/subtraction, multiplication, division, square root calculations, the number of memory read/write operations, and the number of comparisons. Based on information from the Zynq 7000 datasheet [46], the number of cycles required by each operation is listed in Table 5. Since the microprocessor runs at 667 MHz, the duration of each clock cycle is approximately 1.5 ns, resulting in the estimated execution times presented in Table 5. Notice that these estimated times closely match the execution times effectively measured and reported in Table 4. It is worth noting that the code executed on the microprocessor could be further optimised to reduce computation time.

Table 5. Estimation of computational cost among S-MPC, DM, and DM-SE strategies, considering Zynq 7000 microprocessor.

Operation	S-MPC		DM		DM-SE	
	Quantity	Cycles	Quantity	Cycles	Quantity	Cycles
Addition/Subtraction	200	200	280	280	280	280
Multiplication	210	633	280	840	280	840
Division	1	18	1	18	1	18
Square root	22	440	24	480	24	480
Memory (read/write)	420	840	450	900	458	916
Comparisons	65	65	70	70	78	78
Estimated Total		2333 cycles		2588 cycles		2612 cycles
Estimated execution time		3.5 µs		3.9 µs		3.92 µs

6. Comprehensive Comparison of Experimental Results and Discussion

The experimental results presented in the previous section give an overview of the performance of the FCS-MPC methods addressed in this work. Waveform details are provided considering some operation points. Then, this section presents a comprehensive

performance assessment of the FCS-MPC methods providing a complete overview of the advantages and limitations of each method in a broader range of operating conditions.

In order to provide this comprehensive performance assessment, experimental results were collected and organised considering three different rotor speeds (1000 rpm, 2000 rpm, and 3000 rpm) and seven different load torques (1 Nm, 1.5 Nm, 2 Nm, 2.5 Nm, 3 Nm, 3.5 Nm, and 4 Nm). This approach results in a total of 84 experimental tests, the results of which are summarised in Figure 9, and in Table 6 for convenience.

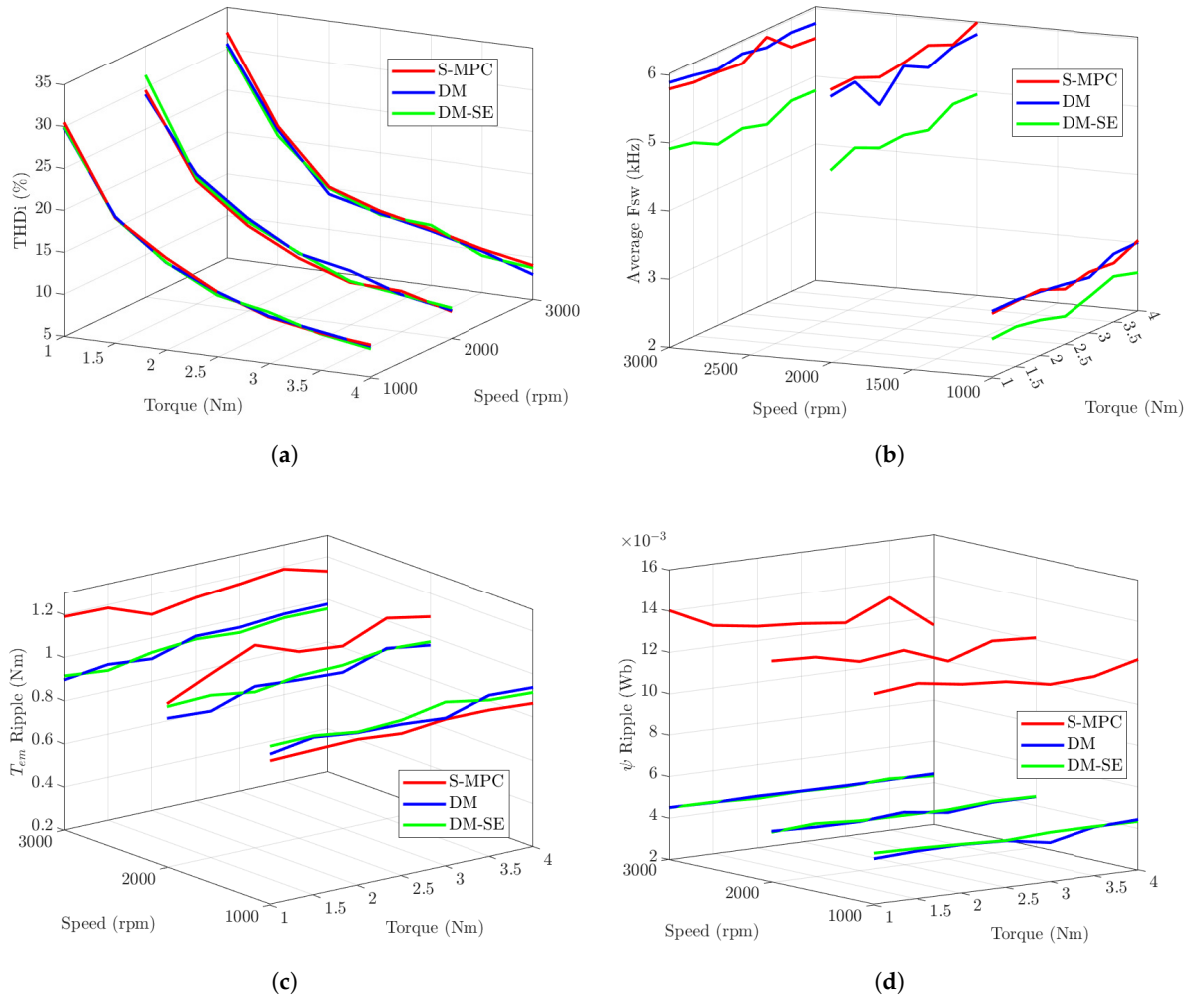

Figure 9. Performance comparison between S-MPC, DM, and DM-SE methods for several speeds and torque load: (**a**) total harmonic distortion (THDi) of current in phase *a*; (**b**) average switching frequency; (**c**) torque ripple; (**d**) flux ripple.

Figure 9a shows an exponential improvement in THDi as the load torque increases. This behaviour is consistent among the three discrete speed points and results in similar THDi values among all FCS-MPC strategies for all operating points tested. It is important to note that the current ripple depends on the dc-link voltage, sampling frequency, and inductance values, which, except for the switching frequency, are constant values. Then the current ripple tends to show a consistent pattern. Since the THDi is a relative measure between the fundamental current component and the current harmonics, which depends on the ripple, the THDi decreases due to an increase in the fundamental component of the current.

Table 6. Comparison of performance metrics at different torque and speed conditions.

Performance Index	Speed (rpm)	Strategy	1 Nm	1.5 Nm	2 Nm	2.5 Nm	3 Nm	3.5 Nm	4 Nm
Average f_{sw} (kHz)	1000	S-MPC	2.94	2.96	2.97	2.81	2.90	2.86	3.03
		DM	2.98	2.98	2.94	2.88	2.82	3.00	3.01
		DM-SE	2.57	2.59	2.52	2.41	2.53	2.67	2.56
	2000	S-MPC	6.01	6.02	5.86	5.91	6.01	5.85	6.02
		DM	5.91	5.96	5.46	5.87	5.68	5.82	5.84
		DM-SE	4.82	4.99	4.82	4.84	4.75	4.97	4.95
	3000	S-MPC	5.79	5.73	5.72	5.68	5.90	5.59	5.56
		DM	5.89	5.83	5.76	5.82	5.75	5.81	5.78
		DM-SE	4.91	4.84	4.65	4.72	4.61	4.80	4.79
THDi (%)	1000	S-MPC	30.49	19.94	15.97	12.76	10.59	9.52	8.92
		DM	29.83	20.06	15.41	12.76	10.70	9.71	8.75
		DM-SE	29.97	19.92	15.46	12.35	11.20	9.43	8.46
	2000	S-MPC	29.68	19.68	15.16	12.11	10.04	9.85	8.23
		DM	29.18	20.45	16.05	12.66	11.45	9.44	8.37
		DM-SE	31.49	20.05	15.62	12.76	10.20	9.42	8.65
	3000	S-MPC	31.94	21.50	15.11	13.05	11.72	10.19	9.05
		DM	30.60	21.06	14.24	12.76	11.51	9.94	7.96
		DM-SE	30.33	20.37	14.94	12.59	12.19	9.40	8.75
T_{em} Ripple (Nm)	1000	S-MPC	0.87	0.87	0.88	0.86	0.88	0.88	0.86
		DM	0.90	0.93	0.91	0.90	0.89	0.95	0.94
		DM-SE	0.94	0.94	0.91	0.92	0.96	0.92	0.91
	2000	S-MPC	0.96	1.05	1.14	1.07	1.05	1.13	1.09
		DM	0.89	0.88	0.95	0.93	0.92	0.99	0.96
		DM-SE	0.95	0.95	0.92	0.95	0.96	0.99	0.98
	3000	S-MPC	1.19	1.19	1.11	1.14	1.16	1.19	1.13
		DM	0.90	0.92	0.90	0.96	0.96	0.98	0.98
		DM-SE	0.91	0.89	0.93	0.95	0.94	0.96	0.96
ψ Ripple (Wb)	1000	S-MPC	0.0122	0.0124	0.0121	0.0119	0.0115	0.0116	0.0122
		DM	0.0042	0.0043	0.0044	0.0043	0.0039	0.0043	0.0044
		DM-SE	0.0045	0.0045	0.0044	0.0043	0.0044	0.0044	0.0043
	2000	S-MPC	0.0127	0.0126	0.0121	0.0123	0.0115	0.0122	0.0121
		DM	0.0045	0.0044	0.0044	0.0045	0.0042	0.0044	0.0044
		DM-SE	0.0044	0.0045	0.0044	0.0044	0.0044	0.0045	0.0044
	3000	S-MPC	0.0140	0.0130	0.0127	0.0125	0.0123	0.0133	0.0116
		DM	0.0045	0.0045	0.0045	0.0045	0.0044	0.0044	0.0044
		DM-SE	0.0045	0.0045	0.0044	0.0044	0.0044	0.0045	0.0043

The DM-SE method was able to effectively reduce the average switching frequency (F_{sw}) of the VSI by introducing the additional control objective in the conventional DM. Figure 9b summarises these results. The S-MPC and the DM methods showed a tight similarity in the switching frequency. The average switching at the speed of 1000 rpm was approximately half the value for the other speed points (2000 rpm and 3000 rpm). This can be attributed to two main factors (1) at higher speeds, the reference voltage vector in the dq frame rotates faster, requiring more frequent switching actions to accurately track it, and (2) higher speeds induce larger disturbances on the load torque of the prime mover, which is characterised by a pronounced torque ripple. In fact, the current ripple of the silver motor is known to increase significantly with speed. This behaviour has been reported in the literature [47].

As discussed in Section 5, the torque and flux ripples produced by S-MPC are higher than for the other two methods, as corroborated by Figure 9c and Figure 9d, respectively. The torque ripple increases with the rotor speed due to the fact that fewer sampling points

are available to run the FCS-MPC methods within a mechanical revolution when the speed and, consequently, the fundamental frequency of the current increase.

Regarding the flux ripple, mapped in Figure 9d, the S-MPC exhibits threefold higher flux oscillations than the decision-making-based methods. This higher flux ripple also contributes to increasing the torque ripple for the S-MPC method, as shown in Figure 9c. The root cause of the higher flux ripple in the S-MPC method is the lack of granularity in optimising the secondary control objective, which is flux control. In turn, as discussed in [15], this leads to suboptimal control, which is unable to fully address both objectives simultaneously, that is, torque and flux tracking.

7. Conclusions

This paper presented a detailed performance assessment of the direct torque control of PMSM using FCS-MPC methods without weighting factors. The comparison considered several speed and torque operating points to build up a complete panorama of key performance indicators: current THD, torque and flux ripples, average switching frequency, and transient performance.

All methods effectively controlled the machine, exhibiting outstanding dynamic performance, a feature expected of FCS-MPC controllers. The torque settling time was lower than 0.4 ms for all control methods. In addition to the low inductance of the machine under test, the THD values were approximately 8% for all methods at any set speed and at nominal torque load. However, flux and torque ripple metrics yielded the best results for the decision-making methods (DM and DM-SE) due to their additional flexibility in coping with control objectives. However, the S-MPC produced higher torque ripples and notably higher flux ripples due to the intrinsic control structure used in the S-MPC, which first evaluates the primary control objective of tracking the reference torque and, after assessing the flux cost function, with a smaller number of available switching vectors.

The flexibility of the decision-making method in incorporating additional control objectives was tested by adding the switching effort, resulting in the DM-SE method. The inclusion of this additional objective did not influence the performance indicator indices. It resulted in a switching frequency 20% lower than that of conventional decision-making (DM) and S-MPC methods.

Despite the comprehensive comparison among the S-MPC, DM, and DM-SE predictive control strategies presented in this work, future research may investigate the performance of these techniques when incorporating discrete virtual voltage vectors. This approach aims to enhance current waveform quality and reduce total harmonic distortion, as well as flux and torque ripples. Moreover, the modulated FCS-MPC framework could be extended to integrate decision-making mechanisms, potentially improving overall system performance.

Author Contributions: Conceptualisation, J.B. and J.R.; methodology, J.B. and J.R.; software, J.B.; validation, J.B.; formal analysis, J.R., E.Z. and M.R.; investigation, J.B. and J.R.; resources, P.W.; data curation, J.B. and E.Z.; writing—original draft preparation, J.B.; writing—review and editing, J.R., E.Z., M.R., R.M. and P.W.; visualisation, J.B., J.R. and E.Z.; supervision, M.R. and P.W.; project administration, M.R.; funding acquisition, J.B., M.R. and P.W. All authors have read and agreed to the published version of the manuscript.

Funding: This research was partly funded by the National Council for Scientific and Technological Development (CNPq), Brazil, Grant 441715/2023-0; Mato Grosso Research Foundation Grant FAPEMAT.01047/2022; National Research and Development Agency (ANID) through the FONDECYT Regular grant number 1220556 and SERC Chile FONDAP 1523A0006. Additional funding was provided by the Research Project PINV01-743 of the National Council of Science and Technology (CONACYT). Furthermore, the authors acknowledge the International Research Collaboration Fund

2024–2025 from the University of Nottingham A7C200 and Programa de Redução de Assimetrias na Pós-Graduação (PRAPG)—Edital nº 14/2023-DRI-CAPES; ID Number: 046.821.818-15.

Data Availability Statement: The original contributions presented in this study are included in the article. Further inquiries can be directed to the corresponding author(s).

Conflicts of Interest: The authors declare no conflicts of interest.

Abbreviations

The following abbreviations are used in this manuscript:

2L-VSI	TWo-Level Voltage Source Inverter
BEMF	Back Electromotive Force
DM	Decision-Making
DM-SE	Decision-Making MPC with additional control objective to minimise the switching effort
DTC	Direct Torque Control
FCS-MPC	Finite Control Set Model Predictive Control
FOC	Field-Oriented Control
GS-MPC	Generalised S-MPC
MPDSC	Model Predictive Direct Speed Control
MPC	Model Predictive Control
MPTC	Model Predictive Torque Control
PI controller	Proportional–Integral controller
PMSMs	Permanent Magnet Synchronous Motors
S-MPC	Sequential Model Predictive Control
THD	Total Harmonic Distortion
VSIs	Voltage Source Inverters
WFs	Weighting Factors

References

1. Huang, K.; Lin, X.; Wu, T.; Luo, T.; Wang, W.; Liu, T.; Zhang, D. An Extended Model Predictive Control for PMSM with Minimum Ripples and Small Runtimes. *IEEE Trans. Ind. Electron.* **2025**, *72*, 9367–9376. [CrossRef]
2. Blaschke, F. The Principle of Field Orientation as Applied to the New Transvector Closed-Loop Control System for Rotating-Field Machines. *Siemens Rev.* **1972**, *34*, 217–220.
3. Wang, T.; Wang, Y.; Zhang, Z.; Li, Z.; Hu, C.; Wang, F. Comparison and analysis of predictive control of induction motor without weighting factors. *Energy Rep.* **2023**, *9*, 558–568. [CrossRef]
4. Takahashi, I.; Noguchi, T. Take a Look Back Upon the Past Decade of Direct Torque Control [of Induction Motors]. In Proceedings of the IECON'97—23rd International Conference on Industrial Electronics, Control, and Instrumentation, New Orleans, LA, USA, 9–14 November 1997; Volume 2, pp. 546–551. [CrossRef]
5. Rodriguez, J.; Garcia, C.; Mora, A.; Flores-Bahamonde, F.; Acuna, P.; Novak, M.; Zhang, Y.; Tarisciotti, L.; Davari, S.A.; Zhang, Z.; et al. Latest Advances of Model Predictive Control in Electrical Drives—Part I: Basic Concepts and Advanced Strategies. *IEEE Trans. Power Electron.* **2022**, *37*, 3927–3942. [CrossRef]
6. Rodriguez, J.; Garcia, C.; Mora, A.; Davari, S.A.; Rodas, J.; Valencia, D.F.; Elmorshedy, M.; Wang, F.; Zuo, K.; Tarisciotti, L.; et al. Latest Advances of Model Predictive Control in Electrical Drives—Part II: Applications and Benchmarking with Classical Control Methods. *IEEE Trans. Power Electron.* **2022**, *37*, 5047–5061. [CrossRef]
7. Kouro, S.; Perez, M.A.; Rodriguez, J.; Llor, A.M.; Young, H.A. Model Predictive Control: MPC's Role in the Evolution of Power Electronics. *IEEE Ind. Electron. Mag.* **2015**, *9*, 8–21. [CrossRef]
8. Rodriguez, J.; Pontt, J.; Silva, C.A.; Correa, P.; Lezana, P.; Cortés, P.; Ammann, U. Predictive Current Control of a Voltage Source Inverter. *IEEE Trans. Ind. Electron.* **2007**, *54*, 495–503. [CrossRef]
9. Li, T.; Sun, X.; Lei, G.; Guo, Y.; Yang, Z.; Zhu, J. Finite-Control-Set Model Predictive Control of Permanent Magnet Synchronous Motor Drive Systems—An Overview. *IEEE/CAA J. Autom. Sin.* **2022**, *9*, 2087–2105. [CrossRef]
10. Novak, M.; Xie, H.; Dragicevic, T.; Wang, F.; Rodriguez, J.; Blaabjerg, F. Optimal Cost Function Parameter Design in Predictive Torque Control (PTC) Using Artificial Neural Networks (ANN). *IEEE Trans. Ind. Electron.* **2021**, *68*, 7309–7319. [CrossRef]
11. Prajapati, D.; Dekka, A.; Ronanki, D.; Rodriguez, J. High-Performance Sequential Model Predictive Control of a Four-Level Inverter for Electric Transportation Applications. *IEEE J. Emerg. Sel. Top. Ind. Electron.* **2024**, *5*, 253–262. [CrossRef]

12. Vazquez, S.; Rodriguez, J.; Rivera, M.; Franquelo, L.G.; Norambuena, M. Model Predictive Control for Power Converters and Drives: Advances and Trends. *IEEE Trans. Ind. Electron.* **2017**, *64*, 935–947. [CrossRef]
13. Wang, X.; Hu, J.; Garcia, C.; Rodriguez, J.; Long, B. Robust Sequential Model-Free Predictive Control of a Three-Level T-Type Shunt Active Power Filter. *IEEE Trans. Power Electron.* **2024**, *39*, 9505–9517. [CrossRef]
14. Zhang, Y.; Zhang, Z.; Babayomi, O.; Li, Z. Weighting Factor Design Techniques for Predictive Control of Power Electronics and Motor Drives. *Symmetry* **2023**, *15*, 1219. [CrossRef]
15. Karamanakos, P.; Geyer, T. Guidelines for the Design of Finite Control Set Model Predictive Controllers. *IEEE Trans. Power Electron.* **2020**, *35*, 7434–7450. [CrossRef]
16. Nasr, A.; Gu, C.; Buticchi, G.; Bozhko, S.; Gerada, C. A Low-Complexity Modulated Model Predictive Torque and Flux Control Strategy for PMSM Drives Without Weighting Factor. *J. Emerg. Sel. Top. Power Electron.* **2023**, *11*, 1305–1316. [CrossRef]
17. Lin, X.; Huang, W.; Jiang, W.; Zhao, Y.; Zhu, S. Predictive Torque Control for PMSM Based on Weighting Factor Elimination and Fast Voltage Vector Selection. *J. Emerg. Sel. Top. Power Electron.* **2020**, *8*, 3736–3750. [CrossRef]
18. Zhang, Y. ; Zhang, B.; Yang, H.; Norambuena, M.; Rodriguez, J. Generalized Sequential Model Predictive Control of IM Drives with Field-Weakening Ability. *IEEE Trans. Power Electron.* **2019**, *34*, 8944–8955. [CrossRef]
19. Yu, Y.; Zhang, J.; Tian, G.; Liu, G. Alternating Sequential Model Predictive Control of Permanent Magnet Synchronous Machine. In Proceedings of the 2023 IEEE International Conference on Predictive Control of Electrical Drives and Power Electronics (PRECEDE), Wuhan, China, 16–19 June 2023; pp. 1–4. [CrossRef]
20. Davari, S.A.; Norambuena, M.; Nekoukar, V.; Garcia, C.; Rodriguez, J. Even-Handed Sequential Predictive Torque and Flux Control. *IEEE Trans. Ind. Electron.* **2020**, *67*, 7334–7342. [CrossRef]
21. Zhang, K.; Liu, Y.; Yang, Y.; Chen, R.; Zhu, Z.; Garcia, C.; Rodriguez, J. Tolerant Sequential Model Predictive Direct Torque Control of Permanent Magnet Synchronous Machine Drives. *IEEE Trans. Transport. Electrif.* **2020**, *6*, 1167–1176. [CrossRef]
22. Ma, C.; Yao, X.; Li, H.; Vansompel, H.; Garcia, C.; Rodriguez, J.; De Belie, F. A Novel Torque Boundary-Based Model Predictive Torque Control for PMSM Without Weighting Factor. *IEEE J. Emerg. Sel. Top. Power Electron.* **2021**, *9*, 4395–4406. [CrossRef]
23. Rojas, C.A.; Rodriguez, J.; Villarroel, F.; Espinoza, J.R.; Silva, C.A.; Trincado, M. Predictive torque and flux control without weighting factors. *IEEE Trans. Ind. Electron.* **2013**, *60*, 681–690. [CrossRef]
24. Bandy, K.; Stumpf, P. Model predictive torque control for multilevel inverter fed induction machines using sorting networks. *IEEE Access* **2021**, *9*, 13800–13813. [CrossRef]
25. Chebaani, M.; Ebeed, M.; Abdellatif, W.S.E.; Elbarbary, Z.M.S.; Nouraldin, N.A. Design and Implementation of an Improved Finite-State Predictive Direct Torque Control for Induction Motor with New Weighting Factor Elimination. *IEEE Access* **2023**, *11*, 58169–58187. [CrossRef]
26. Kusuma, E.; Eswar, K.M.R.; Kumar, T.V. An effective predictive torque control scheme for PMSM drive without involvement of weighting factors. *IEEE Trans. Emerg. Sel. Top. Power Electron.* **2021**, *9*, 2685–2697. [CrossRef]
27. Muddineni, V.P.; Bonala, A.K.; Sandepudi, S.R. Enhanced weighting factor selection for predictive torque control of induction motor drive based on VIKOR method. *IET Electr. Power Appl.* **2016**, *10*, 877–888. [CrossRef]
28. Rojas, C.A.; Rodriguez, J.R.; Kouro, S.; Villarroel, F. Multiobjective fuzzy-decision-making predictive torque control for an induction motor drive. *IEEE Trans. Power Electron.* **2017**, *32*, 6245–6260. [CrossRef]
29. Muddineni, V.P.; Sandepudi, S.R.; Bonala, A.K. Finite control set predictive torque control for induction motor drive with simplified weighting factor selection using TOPSIS method. *IET Electr. Power Appl.* **2017**, *11*, 749–760. [CrossRef]
30. Vujji, A.; Gupta, Y.B.S.S.; Dahiya, R.; Bhaskar, M.S.; Khan, B. Experimental Verification for Cost Function Optimization Using TOPSIS Approach for Predictive Control of Surface Mounted PMSM. *IET Power Electron.* **2023**, *16*, 948–960. [CrossRef]
31. Bhowate, A.; Aware, M.; Sharma, S. Predictive Torque Control with Online Weighting Factor Computation Technique to Improve Performance of Induction Motor Drive in Low Speed Region. *IEEE Access* **2019**, *7*, 42309–42321. [CrossRef]
32. Muddineni, V.P.; Bonala, A.K.; Sandepudi, S.R. Grey relational analysis-based objective function optimization for predictive torque control of induction machine. *IEEE Trans. Ind. Appl.* **2021**, *57*, 835–844. [CrossRef]
33. Vujji, A.; Dahiya, R. Enhancement of weighting coefficient selection using grey relational analysis for model predictive torque control of PMSM drive. *Distrib. Gener. Altern. Energy J.* **2023**, *38*, 1433–1454. [CrossRef]
34. Muddineni, V.P.; Bonala, A.K.; Sandepudi, S.R. Improved Weighting Factor Selection for Predictive Torque Control of Induction Motor Drive Based on a Simple Additive Weighting Method. *Electr. Power Compon. Syst.* **2017**, *45*, 1450–1462. [CrossRef]
35. Vujji, A.; Dahiya, R. Real-Time Implementation for Improvement of Weighting Coefficient Selection Using Weighted Sum Method for Predictive Torque Control of PMSM Drive. *Arab. J. Sci. Eng.* **2023**, *48*, 6489–6505. [CrossRef]
36. Zerdali, E.; Altıntaş, M.; Bakbak, A.; Meşe, E. Computationally efficient predictive torque control strategies without weighting factors. *Turk. J. Electr. Eng. Comput. Sci.* **2022**, *30*, 2554–2567. [CrossRef]
37. Zerdali, E.; Rivera, M.; Wheeler, P.; Gallardo, S.T. Predictive Direct Speed Control of PMSM Without Weighting Factors. In Proceedings of the IEEE 8th Southern Power Electronics Conference and 17th Brazilian Power Electronics Conference (SPEC/COBEP), Florianópolis, Brazil, 26–29 November 2023; pp. 1–6.

38. Liu, R.; Li, H.; Zhou, Y.; Yang, L.; Huang, J. Equivalent Weighting Factor-Based Model Predictive Torque Control of SMPMSM. *IEEE J. Emerg. Sel. Top. Power Electron.* **2023**, *11*, 4808–4817. [CrossRef]
39. Xie, H.; Novak, M.; Wang, F.; Dragicevic, T.; Rodríguez, J.; Blaabjerg, F.; Kennel, R.; Heldwein, M.L. An Ensemble Regulation Principle for Multiobjective FCS-MPC of IM Drives. *IEEE Trans. Power Electron.* **2023**, *38*, 3069–3083. [CrossRef]
40. Xie, H.; Novak, M.; Wang, F.; Dragicevic, T.; Rodríguez, J.; Blaabjerg, F.; Kennel, R.; Heldwein, M.L. Cooperative Decision-Making Approach for FCS-MPC Without Weighting Parameters. *IEEE Trans. Ind. Electron.* **2024**, *71*, 4495–4506. [CrossRef]
41. Zerdali, E.; Rivera, M.; Yildiz, R.; Wheeler, P.; Rodriguez, J. Weighting Factor Elimination Techniques for Model Predictive Control of AC Machines: A Comparison. In Proceedings of the 2025 IEEE 19th International Conference on Compatibility, Power Electronics and Power Engineering (CPE-POWERENG), Antalya, Türkiye, 20–22 May 2025; pp. 1–6. [CrossRef]
42. Norambuena, M.; Rodriguez, J.; Zhang, Z.; Wang, F.; Garcia, C.; Kennel, R. A Very Simple Strategy for High-Quality Performance of AC Machines Using Model Predictive Control. *IEEE Trans. Power Electron.* **2019**, *34*, 794–800. [CrossRef]
43. Kazerooni, M.; Hamidifar, S.; Kar, N.C. Analytical modelling and parametric sensitivity analysis for the PMSM steady-state performance prediction. *IET Electr. Power Appl.* **2013**, *7*, 586–596 . [CrossRef]
44. Galassini, A.; Lo Calzo, G.; Formentini, A.; Gerada, C.; Zanchetta, P.; Costabeber, A. UCube: Control platform for power electronics. In Proceedings of the 2017 IEEE Workshop on Electrical Machines Design, Control and Diagnosis, WEMDCD 2017, Nottingham, UK, 20–21 April 2017; pp. 216–221. [CrossRef]
45. Wilhelm, R.; Engblom, J.; Ermedahl, A.; Holsti, N.; Thesing, S.; Whalley, D.; Bernat, G.; Ferdinand, C.; Heckmann, R.; Mitra, T.; et al. The worst-case execution-time problem—overview of methods and survey of tools. *ACM Trans. Embed. Comput. Syst.* **2008**, *7*, 36. [CrossRef]
46. Xilinx Inc. *Zynq-7000 SoC Technical Reference Manual*; UG585 (v1.14); Xilinx: San Jose, CA, USA, 2023.
47. Tang, M.; Gaeta, A.; Formentini, A.; Zanchetta, P. A Fractional Delay Variable Frequency Repetitive Control for Torque Ripple Reduction in PMSMs. *IEEE Trans. Ind. Appl.* **2017**, *53*, 5553–5562. [CrossRef]